SEMI-ANALYTICAL SPRING-IN ANALYSIS TO COUNTERACT CFRP MANUFACTURING DEFORMATIONS BY TOOL COMPENSATION

Erik Kappel*, Daniel Stefaniak*, Christian Hühne*
*** German Aerospace Center DLR, Institute of Composite Structures ans Adaptive Systems**
D-38108, Braunschweig, Germany
mail: erik.kappel@dlr.de, phone+49-(0)531-295-2398

Keywords: *composite manufacturing, manufacturing deformations, spring-in, compensation, CFRP*

Abstract

Within this paper an excerpt of a comprehensive experimental test program is presented which accounts for the main drivers of spring-in deformations. Therein, it is focused on the effect of layup and part-radii changes on the occurring spring-in deformations of fully cured parts. By means of full-field geometrical measurements, the thermal fraction of the spring-in deformation is experimentally quantified. Experimental findings are validated using an analytical approach by Radford. Furthermore, a new semi-analytical shell-element-based simulation strategy is proposed which focuses on the prediction of manufacturing induced part deformations. Therein, necessary parameters are derived from simple test specimens, which lead to a comparably simple procedure, which should support tool designers in their daily work. Finally, the developed approach is applied to a C-profile part and experimentally validated.

1 Problem's Topicality

Rapidly increasing manufacturing cadences for modern aircrafts are accompanied by a strong demand for efficient simulation methods accounting for the particularities of the composite manufacturing process. First-time-right fabrication is aspired, as it is one essential key to reduce overall costs, due to the avoidance of cost intensive and time consuming manual (re)work.

Currently, manufacturing induced deformations are still a challenge for *carbon fiber reinforced plastics* (CFRP) manufacturers, as those undesired deviations from the nominal shape lead to increased scrap rates and/or additional difficulties within the assembly process. A connection of deformed parts e.g., can lead to a massive increase of the part's internal stress level which deteriorate the part's performance. Figure 1 illustrate that schematically.

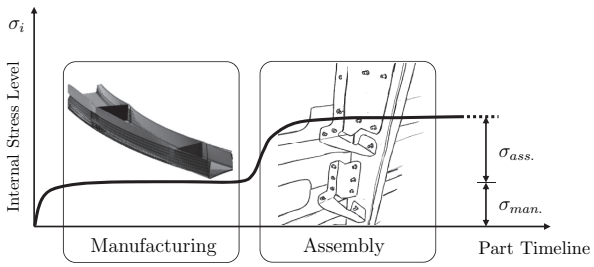

Fig. 1 Undesired part deformations lead to significant assembly stresses $\sigma_{ass.}$ (C-spar taken from [6])

In accordance with Fernlund et al. [1], this paper distinguishes between two main fractions of manufacturing deformations which are spring-in and warpage. The former one is induced by the composite's anisotropic properties and predominant for parts with angled cross-sections. Warpage is induced by tool-part interaction due to a mismatch in *coefficients of thermal expan-*

sion (CTE) of tool and part and/ or due to gradients in *fiber volume fraction* (V_f) .

The present paper focuses on spring-in deformations, as experimental investigations, conducted at the DLR [2, 3], reveal that warpage is only relevant for a particular group of composite structures.

Reflecting the anisotropic mechanical and thermal properties of an *unidirectional* (UD) CFRP lamina and the resin's significant shrinkage during current high-temperature manufacturing processes, it becomes obvious that manufacturing deformations are widely inevitable for CFRP laminates.

But, however, own experimental investigations and experimental work stated in the literature [1, 4, 5, 9, 10], suggests that the magnitude of expectable angle changes of curved sections is rather limited. Nevertheless, those small changes in curved sections can lead to massive part deformations, depending on the part's scale and shape.

Tool geometry compensation represents a promising approach with good industrial applicability to counteract manufacturing deformations, as it can be easily integrated into the product-development-chain. However, a reliable tool compensation strategy demands knowledge of expectable part deformations - prior to manufacturing.

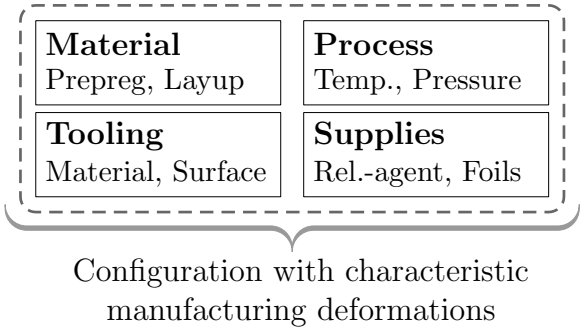

Fig. 2 Configuration specific manufacturing deformations

Considering a common manufacturing scenario, where a certain CFRP material is fabricated on a certain tool(-material) with a certain manufacturing process and a certain bagging arrangement, it is physically reasonable that obtained deformations are characteristic and reproducible for that particular configuration. Consequently, it is assumed that the measurement of manufacturing deformations of appropriate test specimens can provide sufficient and representative information about the configuration's deformation characteristics what is schematically illustrated in Figure 2.

Thus, this paper pursues a semi-analytical strategy to overcome drawbacks of existing micro-level simulation strategies (e.g. [11, 12]) as those are characterized by high parameter determination efforts. Geometrical measurement of manufacturing induced deformations on specimen level are used for the derivation of corresponding equivalent simulation parameters applicable on part level.

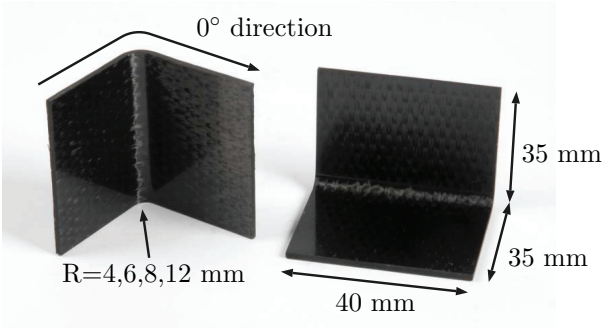

Fig. 3 Geometric properties of the L-profile specimens and 0° orientation

The global aim of this strategy is to provide a straightforward simulation process, demanding as few parameters as possible, which can support tool-designers in their daily work. Simple L-profiles depicted in Figure 3, similar to that ones used by Spröwitz et al. [5], are suitable for the aforementioned approach as they can easily be fabricated and analyzed.

Within the following, an excerpt of a comprehensive experimental L-profile-based test-program is presented. The main drivers of spring-in deformations and the quantification of fractions due to thermal anisotropy and due to chemical shrinkage are within the scope of the conducted investigations. Experimental results are checked for plausibility by comparison with an-

alytical calculations based on an approach proposed by Radford [10]. Subsequently, a new semi-analytical simulation strategy is presented, which uses deformation measurements on specimen level for the derivation of equivalent simulation parameters, which can be used on part and component level. The main advantage of that approach is the use of conventional shell elements, which simplifies modeling massively. Finally, the developed approach is applied and experimentally validated to a simple sample-case.

2 Experimental Investigations

Within this section the effect of part-radius and layup on the spring-in behavior for a 90° L-profile is investigated. Therefore, 64 specimens have been manufactured on an aluminum male-tooling, which provides four different male-radii (R = 4, 6 , 8, 12 mm). Four different configurations, each characterized by a different layup, have been fabricated within four autoclave runs. Table 1 shows the different configurations. It should be noted that the 0°-direction is oriented in circumferential direction of the specimens as shown in Figure 3.

Name	Layup	Thickness [mm]
C1	$[0]_8$	1.50
C2	$[0,90]_s$	0.75
C3	$[45,-45,90,0]_s$	1.50
C4	$[45,-45]_s$	0.75

Table 1 Layup of investigated specimen configurations

The laminates investigated in this study are composed of UD plies of Hexply®8552/35%/194/AS4 prepreg material with a nominal cured ply thickness of 0.185 mm. All specimens have been fabricated using the same bagging setup, depicted in Figure 4, following the *manufacturer's recommended cure cycle* (MRCC) [7]. Prior to each manufacturing run two coats of Chem-Trend Chemlease® liquid release agent have been applied on the tool in order to assure constant tool-surface properties. Spring-in deformations of the specimens are

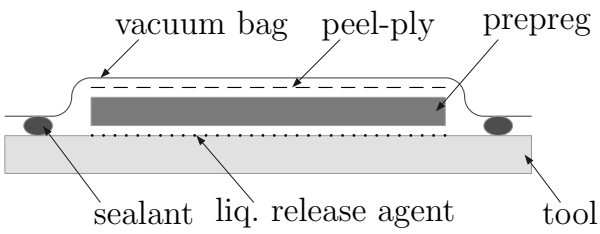

Fig. 4 Bagging setup used for all specimens

measured using a high resolution 3D full field GOM Atos measurement system. Therein, best-fit planes are assigned based on manually selected areas at the flanges of the obtained point cloud. Evaluation of the angle between

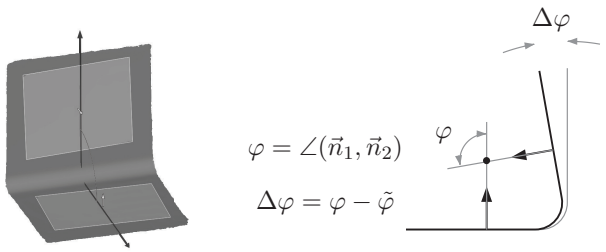

Fig. 5 Point-cloud based measurement technique

both plane normals allow the derivation of the part's spring-in angle as depicted in Figure 5. In contrast to Albert and Fernlund [1] no flange warpage was measurable for the manufactured specimens in this study. Multiple measurements of one test specimen reveal a standard deviation of the measured spring-in angle of $s_{mes} < 0.01°$ which is sufficiently accurate.

2.1 Spring-In Deformations of Various Layups

The measured spring-in angles of the four different configurations, given in Table 1, are shown in Figure 6. Measured values reveal clear differences between the single layups, whereas obtained angles within one configuration are widely comparable. As R12 specimens of the C4 configuration show conspicuous divergence from other specimens of that configuration those results are excluded from the following evaluation.

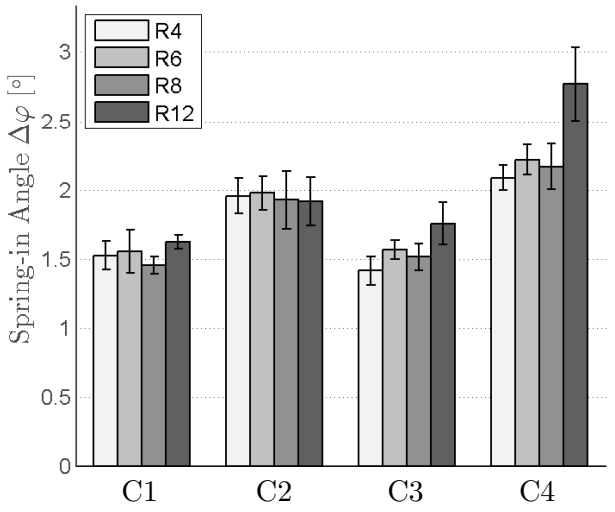

Fig. 6 Measured spring-in angles of all configurations

Regarding all other specimens although their laminate differs significantly, gives an average spring-in angle $\Delta\bar{\varphi}$ of 1.78° with a standard deviation of $S_{\Delta\bar{\varphi}}$ of 0.27°. Configuration C3 with it's quasi-isotropic layup show an average $\Delta\bar{\varphi}_{C3}$ of 1.56° and a standard deviation of 0.16°. No consistent dependency of the spring-in angle from the tool-radius is obtained for all configurations. Only a slight increase for 12 mm radius for configurations C2 and C3 is conspicuous. However, similar tendencies for increasing tool radii have been reported earlier by Hamamoto [8]. A gradient in V_f in circumferential direction due to corner thinning would be a possible explanation. But, however, V_f measurements on selected specimens along the circumferential direction reveal no gradient in the curved area of the L-profiles.

Regarding configuration C4, which corresponds to a $[45,-45]_s$ layup, the massive increase for the R12 specimens is conspicuous. Indicated by the comparably large standard deviation within the group of four specimens and supported by the finding of Fernlund et al. [9], it is assumed that the missing plies in circumferential direction lead to a sensitive part behavior.

Nevertheless, experimental findings presented in the preceding support the aforementioned statement, that expectable spring-in deformations are within a small range. For the experiments presented above that range is $1.4° < \Delta\varphi < 2.2°$.

2.2 Experimental Quantification of Spring-In Fractions

It is widely accepted that the spring-in angle is composed of one fraction induced by thermal anisotropy of the composite laminate and one fraction induced by the resin's chemical shrinkage during the curing process (e.g. [1]).

However, opinions about the size of each fraction strongly diverge. Knowing that, chemical fractions have residual character and thermal fraction are elastic, reheating a specimen enables the determination of the thermal spring-in fraction.

$$\Delta\varphi = \Delta\varphi_{th} + \Delta\varphi_{ch} \tag{1}$$

Therefore, one specimen of each configuration (Radius R6) has been heated with controllable hot-plate, while multiple measurements of the changing deformation state are performed using the technique described above. Therein the

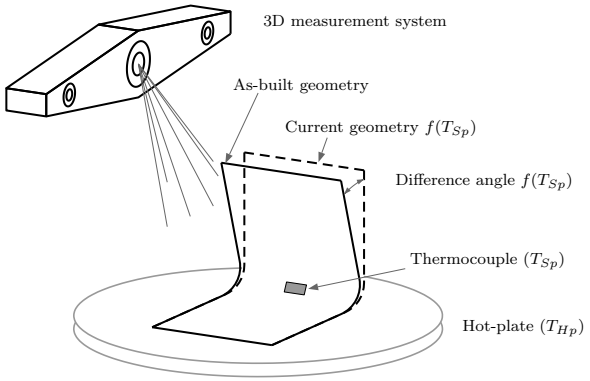

Fig. 7 Measurement setup capturing part deformations due to heating

temperature range of the experiments has been $24°C < T < 130°C$. In order to compensate radiation and convection effects ($T_{Sp} < T_{Hp}$), part temperature is controlled using a thermocouple applied to the inner L-profile surface. Figure 7 shows the experimental setup schematically.

As the thermo-elastic spring-in fraction φ_{th} changes during the heating of the L-profile, the

evaluation of multiple optical measurements allows an interpolation of the spring-in angle $\Delta\varphi$ as a function of temperature. Figure 8 shows a similar experiment during the measurement. The

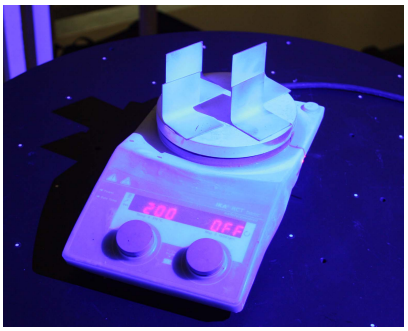

Fig. 8 Specimens applied on the hot-plate during a measurement

evaluation of the different measurements can be interpolated linearly. From further experiments it is known that an extrapolation up to 180°C is allowed.

Assuming that the composite is fully cured at the end of the 180°C hold the difference between $\Delta\varphi_{th,20°C} - \Delta\varphi_{th,180°C}$ gives the thermo-elastic fraction of the spring-in angle $\Delta\varphi_{th}$. Division by

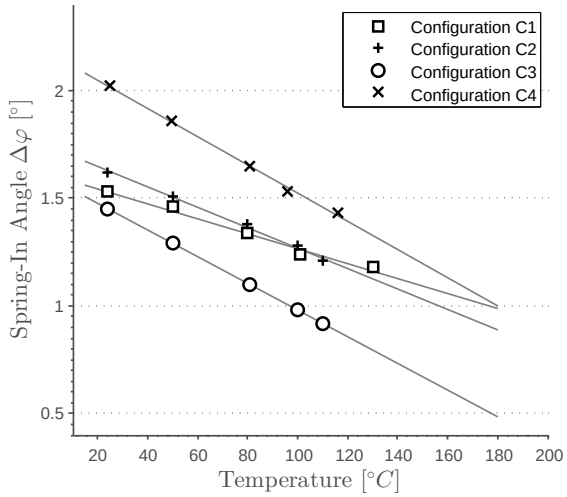

Fig. 9 Linear interpolation of the Spring-in angle $\Delta\varphi$ as a function of temperature for each configuration (Radius R6)

the total spring-in angle $\Delta\varphi$ gives the percentage of the thermal spring-in fraction. Figure 9 shows the experimental findings for all investigated configurations, whereas Table 2 lists thermal fractions as well as percentages.

Name	$\Delta\varphi_{th}$ [°]	$\Delta\varphi_{th}/\Delta\varphi$ [%]
C1	0.56	36.6
C2	0.75	46.4
C3	0.99	68.4
C4	1.06	52.3

Table 2 Experimentally obtained thermal fraction of the spring-in angle $\Delta\varphi_{th}$

The thermal fraction of 68.5 % for the configuration C3 is remarkably high. As it has not been remeasured it should be treated with caution.

3 Analytical Validation

In order to substantiate the preceding experimental findings an analytical study has been performed, wherein equation 2 is used, which has been proposed by Radford [10].

$$\Delta\varphi = \frac{\varepsilon_T - \varepsilon_R}{1+\varepsilon_R} \cdot \tilde{\varphi} \tag{2}$$

Therewith, the angle change $\Delta\varphi$ of a constantly curved section is derived with use of the anisotropic strain components in thickness (radial) direction ε_R and circumferential (tangential) direction ε_T and the initial section angle $\tilde{\varphi}$.

As the laminate properties depend significantly on the layup and the V_f, those parameters are in the focus of the conducted study. While the thermal expansion parameters of the composite can be easily derived using *classical laminate thoery* (CLT) the corresponding resin shrinkage induced strain components need further attention. Therefore, the shrinkage of the isotropic resin needs to be transfered to corresponding laminate shrinkage properties.

Regarding a cuboid with the edge-lengths a,b,c the volumetric shrinkage ΔV can be derived based on strain components in edge directions as shown in equation 3.

$$\Delta V = \varepsilon_a\varepsilon_b\varepsilon_c + \varepsilon_a\varepsilon_b + \varepsilon_a\varepsilon_c + \varepsilon_b\varepsilon_c + \varepsilon_a + \varepsilon_b + \varepsilon_c \tag{3}$$

For a UD ply, it is assumed that the resin's volumetric chemical shrinkage results in a homogeneously shrinkage in transverse direction $\varepsilon_b = \varepsilon_c = \varepsilon^*$ and no shrinkage in fiber direction $\varepsilon_a = 0$.

That assumption is based on the fact that resin shrinkage mainly generates shortly after passing the gelation-point where the resin stiffness is significantly lower than the fiber stiffness. Therefore, the high fiber stiffness prohibits shrinkage induced strain in fiber direction. As only the resin fraction of the cuboid volume shrinks the term $(1 - V_f)$ needs to be introduced into equation 4 in order to derive equivalent strains for a composite material. Consequently, equation 3 can be simplified and rearranged to:

$$\varepsilon^* = -1 + \sqrt{1 + (1 - V_f)\,\Delta V} \qquad (4)$$

Thus, strains due to thermal expansion and due to chemical shrinkage in local UD ply coordinates are denoted as $\underline{\varepsilon}_{th} = (\alpha_1, \alpha_2, 0)^T \cdot \Delta T$ and $\underline{\varepsilon}_{ch} = (0, \varepsilon^*, 0)^T$ respectively. Based on the preceding, homogenized parameters are derived according to equation 5, whereas $\bar{\underline{\varepsilon}}$ denote strain in laminate coordinate system.

$$\left\{ \begin{array}{c} \bar{\underline{\varepsilon}}_{th,lam} \\ \bar{\underline{\varepsilon}}_{ch,lam} \end{array} \right\} = \underline{\underline{A}}^{-1} \cdot \sum_{k=1}^{N} \underline{\underline{\bar{Q}}}_k \cdot t_k \cdot \left\{ \begin{array}{c} \bar{\underline{\varepsilon}}_{th} \\ \bar{\underline{\varepsilon}}_{ch} \end{array} \right\} \qquad (5)$$

While tangential strain components used within equation 2 can be derived based on CLT, it is assumed, that the strain components in thickness direction ε_R are equal to the UD ply properties in transverse direction, as both are resin-dominated. Figure 10 illustrates the origins of the utilized parameters. The resin's volumetric shrinkage and the fiber volume fraction is assumed to $\Delta V = -3.75$ % and $V_f = 50$ % within the following comparison of analytical and experimental findings. Table 3 lists the fiber and resin material parameters used within this study.

Rules of mixture are taken from [17, 18, 19].

Applying the analytical model to the C2 laminate reveal good agreement with the experimental findings presented above. The analytically derived thermal fraction of the spring-in angle $\Delta\varphi_{th}$

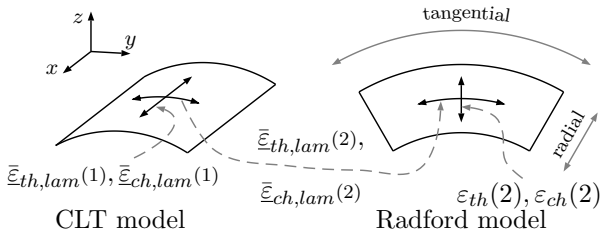

Fig. 10 Origins of the strain components used with the Radford model

Parameter	Value	Unit
E_{f1}	231.0	GPa
E_{f2}	21.0	GPa
ν_{12f}	0.25	-
G_{12f}	28.0	GPa
α_{f1}	−0.63	ppm/K
α_{f2}	7.2	ppm/K
E_R	4670	MPa
ν_R	0.25	-
α_R	65	ppm/K

Table 3 Fiber and resin properties used within the study (taken from [14, 15, 16])

is obtained to 44.4 %, and the total spring in angle $\Delta\varphi$ is obtained to 1.42°. Comparing those results with the experimental findings given in Table 2 reveal deviations of 2 % in the thermal fraction and 13 % in the total spring-in angle.

The spring-in angle and it's fractions as a function of V_f is shown in Figure 11.

Considering the uncertainties of the used material parameters and the experimental setup the accordance between analytical prediction and experimental findings is satisfying. Nevertheless, further experimental tests are desirable to improve the developed model.

4 Numerical Model

The preceding experimental and analytical investigations clearly show that CFRP laminates, composed of differently aligned UD lamina, tend to deform during manufacturing due to the material's anisotropy.

Following the assumption that a certain

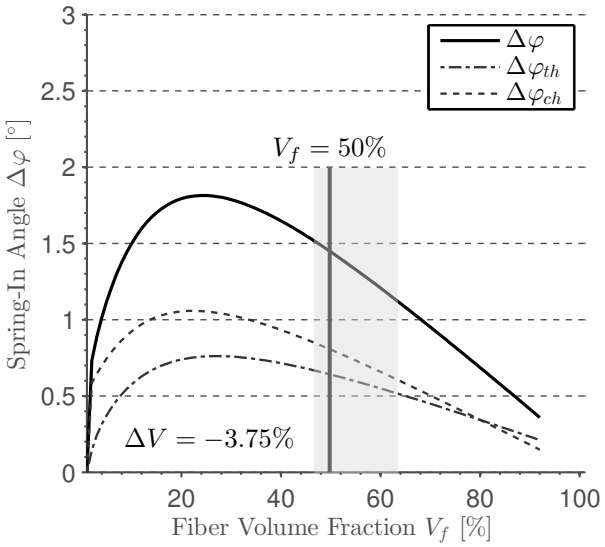

Fig. 11 Spring-in angle calculation as a function of V_f for a $[0,90]_s$ cross-ply laminate

manufacturing configuration results in a certain spring-in deformation, as schematically depicted in Figure 2, measured deformations on test specimen level allow the derivation of corresponding parameters for FE simulation on part-level.

Therefore, a new semi-analytical simulation strategy has been developed, which uses a shell modeling approach, in order to overcome the drawbacks of fine solid element modeling of current numerical approaches.

It should be noted that the approach focuses solely on part deformations as this parameter is essential for the derivation of tool-compensation countermeasures. Within the simulation strategy, measured deformations on L-profile level are transfered to an equivalent mechanical load. The model follows the basic considerations of a bi-metal, as ply-wise inhomogeneous in-plane strains lead to a resulting bending moment $\underline{M}^*$ as given by equation 6.

$$\underline{M}^* = \sum_{k=1}^{n} \underline{\underline{\bar{Q}}}_k \cdot \underline{\bar{\varepsilon}}^*_k \cdot \frac{1}{2}(h_k^2 - h_{k-1}^2) \qquad (6)$$

Focusing on manufacturing deformations and therefore disregarding other mechanical loads allows the derivation of curvature change $\partial\varphi/\partial s$ due to the bending moment $\underline{M}^*$ for a simply curved geometry as shown in equation 7. It should be noted that this simplification is for sake of clarity only and it is not a general limitation of the derived model.

$$(\partial\varphi/\partial s, 0, 0)^T = \underline{\underline{D}}^{-1} \cdot \underline{M}^* \qquad (7)$$

The integration along the arc length gives the angle change $\Delta\varphi$, given by equation 8, as a function of the nominal section angle $\tilde{\varphi}$, the nominal radius in direction of curvature $R_{0,\varphi}$ and a modeling parameter, which is illustrated in Figure 12.

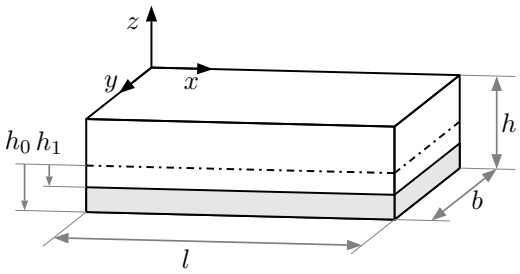

Fig. 12 Illustration of the modeling parameter which is part equation 8

$$\Delta\varphi = \tilde{\varphi} \cdot R_{0,\varphi} \cdot \frac{6\Delta T\,\alpha_\varphi \left(h_k^2 - h_{k-1}^2\right)}{h^3} \qquad (8)$$

For the sake of convenient modeling, modification strains $\bar{\varepsilon}^*$ are considered as thermal strains within the FE tool, whereas $\bar{\varepsilon}^* = \bar{\alpha}^* \Delta T$ is introduced. Rearranging of equation 8 gives the expansion parameter in direction of curvature α_φ as a function of nominal geometric parameters of the measured specimen, measured spring-in deformations of the specimen and a modeling term. This term is related to the thickness of the manipulated area within the FE calculation.

$$\alpha_\varphi = \frac{\Delta\varphi}{\tilde{\varphi}} \cdot \frac{1}{R_{0,\varphi}\Delta T} \cdot \frac{h^3}{6\left(h_k^2 - h_{k-1}^2\right)} \qquad (9)$$

It should be noted that the parameter derivation is directly linked to the underlying simulation model and cannot be regarded separately.

Model Application

In order to substantiate the suitability of the developed model for tool compensation issues, the

model has been experimentally validated for a simple C-profile. Therefore, two different tools have been fabricated, whereas one with nominal geometry and one with compensated geometry. As a kind of worst-case scenario, the layup $[45, -45]_{4s}$ is used for the experimental study, as it shows the largest spring-in angle on specimen-level of $\Delta\varphi = 2.22°$. According to equation 9, the

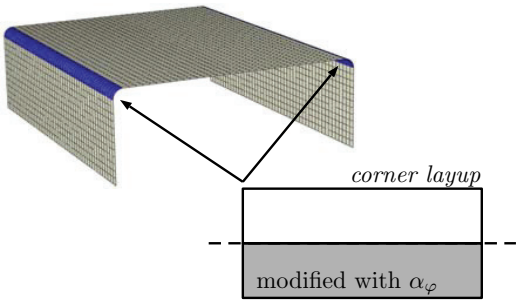

Fig. 13 FE mesh of the nominal geometry with modified corner layup

modification parameter α_φ in direction of curvature is derived to $\alpha_\varphi = 50.704$ ppm/K, when a temperature load of $\Delta T = -160$K , similar to a cool down of a 180°C resin system to room temperature, is assumed. The simulational model is based on the nominal tool surface with the geometrical parameters $\tilde{\varphi} = 90°$ and the section radius $R_{0,\varphi} = 6$ mm, which is transfered from the CAD tool to the FE tool.

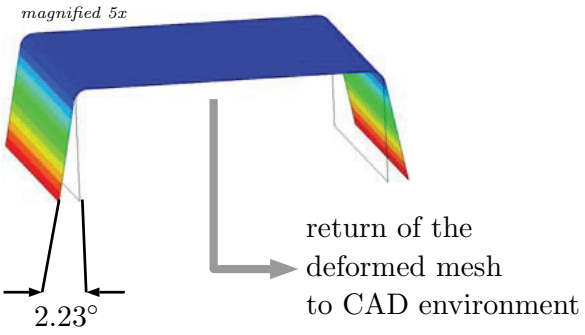

Fig. 14 Spring-in compensated part shape (magnified 5x) and nominal geometry (transparent)

As shown in Figure 13, the half of the corner layup is modified. Therefore, α_φ is assigned in direction of curvature by use of orthotropic expansion properties. The application of the thermal load leads to a deformation of the curved area. In context of a compensation task the sign of the thermal load is changed. Thus, a spring-in compensation is achieved, which is shown in Figure 14. Using the derived node translations of the FE model within the CAD environment allows an update of the nominal tool surface. The compensation procedure outlined in the preceding has been used to design the compensated tooling geometry depicted in Figure 15. Geometrical measurement of the fabricated specimens reveal a complete reduction of the spring-in angle.

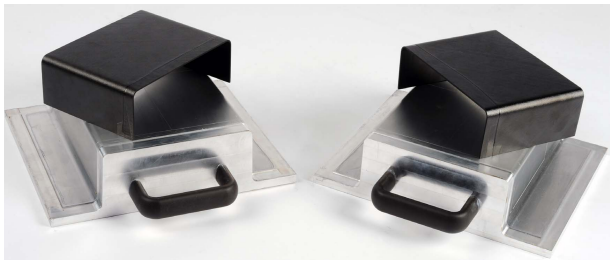

Fig. 15 Nominal and compensated tooling with fabricated C-profile

5 Summary

An excerpt of a comprehensive experimental study performed by the DLR is presented, accounting for the effects of varying layups and part radii on spring-in deformations. Therefore, a set of 64 L-profile test specimens with four different layups has been autoclave-fabricated out of 8552/AS4 prepreg material, whereas the 180°C MRCC is used. A 3D full-field measurement technique is used to measure spring-in deformations of the specimens. Experimental results reveal that the spring-in angle is widely independent from part radius but varies for different layups. However, the range of obtained spring-in angles is very limited $1.4° < \Delta\varphi < 2.2°$, which is in accordance with the literature. In order to quantify the thermal fraction φ_{th} of the total spring-in, one specimen of each layup has been reheated using a controllable hot plate. The aforementioned measurement technique has been used to measure the changing spring-in angle

for different specimen temperatures. A linear thermo-elastic relation of the spring-in angle is obtained, whereas slopes are different for each layup. The thermal fraction of the spring-in varies between 36.6 % and 68 %, dependent on the layup. An analytical model proposed by Radford has been used to verify the experimental findings for a cross-ply laminate. Good agreement is found for an assumed total resin cure shrinkage of -3.75 %. Finally a new simulation strategy focusing solely on part deformation is presented, which should support tool designers in their daily work. The main innovation of the new strategy is that cost intensive parameter derivation, as they are necessary for current numerical approaches, is substituted by an analytical parameter calculation based on fabricated simple L-profile test specimens. Furthermore, it utilizes simple shell element modeling within the FE environment, which is a significant advantage in contrast to existing approaches. The developed approach has been applied and experimentally validated to a simple test-case. Therein, the spring-in angle could be successfully compensated.

6 Outlook

Within future work, the potential of the new simulation strategy will be experimentally and numerically validated for doubly-curved and more-integral structures. Further experimental studies with non-prepreg technologies will be performed, in order to widen the area of applicability and to account for the particularities of different manufacturing procedures such as RFI or RTM e.g.. Furthermore, a promising measurement technique will be investigated striving for a more simplified and thus cheaper way of the parameter determination. In addition, the presented approach will be supplemented by a second calculation step, in order to allow a quantification of induced stresses due to assembly $\sigma_{ass.}$.

References

[1] C.Albert and G.Fernlund. *Spring-In and warpage of angled composite laminates* Composite Science and Technology, 2002, Volume 64, pp. 1895-1912

[2] E.Kappel, D.Stefaniak, T.Spröwitz and C.Hühne *A semi-analytical simulation strategy and its application to warpage of autoclave-processed CFRP parts* Composites: Part A, 2011, Volume 42, pp. 1985-1994

[3] D.Stefaniak, E.Kappel, T.Spröwitz and C.Hühne *Experimental identification of process parameters inducing warpage of autoclave-processed CFRP parts* Composites: Part A, 2012, Volume 43, pp. 1081 - 1091

[4] L.K.Jain, M.Hou, L.Ye and Y.-W.Mai. *Spring-in study of the aileron rib manufactures from advanced thermoplastic composite*. Composites: Part A, 1998 29A, 973-979

[5] T.Spröwitz, J.Tessmer and T.Wille *Thermal aspects for composite Structures - from manufacturing to in-service predictions* ICAS 2008, Proceedings

[6] M.Svanberg *Predictions of Manufaturing Induced Shape Distortions - high performance thermoset composites (PhD Thesis)* Department of Applied Physics and Mechanical Engineering, Luleå University of Technology, 2002

[7] T.Spröwitz, J.Tessmer and T.Wille *Thermal aspects for composite Structures - from manufacturing to in-service predictions* ICAS 2008, Proceedings

[8] A.Hamamoto. *Curing of l-shaped composite parts*. Proceedings of International Symposium on Composite Materials and Structures, pages 1092 - 1097

[9] G.Fernlund, N.Rahman, R.Courdji, M.Bresslauer, A.Poursartip, K.Willden, and K.Nelson. *Experimental and numerical study of the effect of cure cycle, tool surface, geometry and lay-up on the dimensional fidelity of autoclave-processed composite parts*. Composites Part A, 33:341-351, 2002

[10] D.W.Radford *Shape stability in composites (PhD Thesis)* Rensselaer Rolytechnic Institute, 1987

[11] J.M.Svanberg and J.A.Holmberg *Prediction of*

shape distortions, Part 1. FE-implementation of a path dependent constitutive model. Composite Part A: Applied Science and Manufacturing Vol. 35, Issue 6, June 2004, pp 711-721

[12] Q.Zhu and P.H.Geubelle *Dimensional accuracy of thermoset composites: shape optimization*. Journal of Composite Materials, Vol. 36, No. 6, 2002, pp 647-672

[13] K.J.Teoh and K.-T.Hsiao *Improved dimensional infidelity of curve-shaped VARTM composite laminates using a multi-stage curing technique - Experiments and modeling*. Composites: Part A 42 (2011) 762-771

[14] HexCel-Composites. *HexTow AS4* - Product Data, 2009.

[15] S.Pellegrino *Ultra-thin Carbon Fiber Composites: Constitutive Modeling and Applications to Deployable Structures Lectures* California Institute of Technology

[16] M.S.Anghelescu and M.K.Alam *Carbon Foam Tooling for Aerospace Composites* Department of Mechanical Engineering, Ohio University,

[17] R.M.Jones *Mechanics of Composite Materials* Hemisphere, New York, 1975

[18] S.W.Tsai *Theory of Composite Design* Think Composites, Dayton,OH,1992

[19] *Structural Materials Handbook, Volume 1 - Polymer Composites* ESA Publications Division, ESTEC, Noordwijk, 1994

Copyright Statement